Blue InGaN Quantum Well LED Fabrication

Mike Grundmann, Jason Haaheim, Amir Moshar, Joe Summers
Department of Electrical and Computer Engineering, University of California – Santa Barbara

Professor: **Shuji Nakamura**
Date: 5/8/02

Abstract

In this paper we report the successful growth, processing, and characterization of Blue Indium Gallium Nitride (InGaN) Multi Quantum Well (MQW) LEDs, as well as the pertinent theory leading thereto. The samples were Rapid Thermal Annealed (RTA) in different ambient gases (100% N_2, 12% O_2 / 88% N_2), and at different points in the overall fabrication (before processing or after thin Ni/Au contact deposition). The RTA served to activate the p-dopant species (Mg), which resulted in p-type GaN. All of our samples luminesced blue, with general peak wavelengths ranging from 426.7 to 482.9 nm, FWHMs from 20.5 to 33.4 nm, and an output power as high as 363.7 μW for a current of 60 mA. We noted a blue-shift in the peak wavelength with increasing current that we attribute to the Quantum Confined Stark Effect. Contact resistance remains a persistent problem, and values as high as 2.3 MΩ were measured. The highest external quantum efficiency was estimated to be 3.5 %.

I. Background: GaN LED Theory and Operation

Spontaneous emission in semiconductors

In LEDs, light is produced by spontaneous emission, where electrons in the conduction band spontaneously recombine with holes in the valence band to emit photons of equal energy ($E_{electron} - E_{hole} = E_g = h\nu$). The rate of spontaneous emission, R, is proportional to the product of electron and hole concentrations.[1]

$$R = -\frac{dn}{dt} = -\frac{dp}{dt} = Bnp \tag{1}$$

Here, n is the concentration of free electrons, p is the concentration of holes, and B is the bimolecular recombination coefficient. This can also be expressed in terms of the equilibrium carrier concentrations (n_o, p_o).[2]

$$R = B(n_o + p_o)\Delta n(t) \tag{2}$$

The rate of change in concentration, Δn(t), is an exponential with a characteristic rise time equal to the carrier lifetime, and Δn_o is the steady state excess electron concentration.[3]

$$\Delta n(t) = \Delta n_o e^{-B(n_0+p_o)t}, \quad \tau = \frac{1}{B(n_o + p_o + \Delta n)} \tag{3}$$

Role of Defects

Defects in GaN are primarily crystal irregularities caused by growth on an imperfectly matched substrate (Sapphire, SiC). These irregularities trap carriers and produce nonradiative transitions in the form of phonons in the lattice, which reduce the efficiency of the LED. Such recombination through traps or defects is described by the Shockley-Read-Hall recombination rate:[4]

$$R_{sr} = s_r v_{th} N_T \frac{np - n_i^2}{n + p + 2n_i \cosh\left(\frac{\varepsilon_T - \varepsilon_{Fi}}{k_B T}\right)} \tag{4}$$

where, N_T is the trap concentration, v_{th} is the thermal velocity of the carriers, and s_r is the electron/hole capture cross section at the trap level. The lifetime for nonradiative transitions, τ_r, is inversely proportional to this rate. Defects are also sometimes responsible for radiative transitions. The yellow luminescence in p-type GaN arises from vacancies (either Ga or N) which produce deep levels within the band and result in lower-energy radiative emission.

Internal Efficiency

The internal efficiency of an LED is defined as the ratio of photons emitted from the active region to electrons injected into the LED. It is a function of the radiative and nonradiative carrier lifetimes.[5]

$$\eta_{\text{int}} = \frac{\tau_r^{-1}}{\tau_r^{-1} + \tau_{nr}^{-1}} \tag{5}$$

In GaN, the radiative lifetime is much smaller than the nonradiative lifetime, so most carriers can recombine to emit photons before encountering traps. For most calculations in mature material systems, it is acceptable to approximate $\eta_{\text{int}} \sim 1$.[6]

Impurity Doped LED vs Quantum Well LED

In an impurity doped LED, electrons from the n- side of a p-n junction and holes from the p-side are injected across the junction by the application of a forward bias.[7] These minority carriers recombine with majority carriers by spontaneous transitions across the bandgap (see Figure 1).[8]

In a quantum well LED, the electrons and holes injected across the p-n junction become confined within the well, piling up and causing an increase in the concentration of holes and electrons (see Figure 2). The recombination rate is proportional to n*p. Therefore, in a heterostructure LED the amount of radiative recombination is larger than in the case of the impurity doped LED. This leads to an increased number of photons emitted for the same current across the junction.

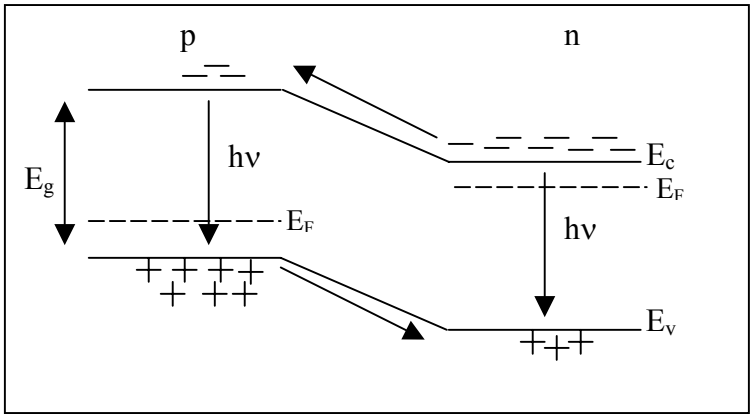

Fig. 1 – injection of minority carriers in a forward biased p-n junction leading to spontaneous emission of photons

Quantum Confined Stark Effects

Piezoelectric fields are formed when materials with different lattice constants come together at a junction. These electric fields are a result of bond stress between the materials, which alter the optical properties of the InGaN LEDs. This is known as the Quantum Confined Stark Effect (QCSE).[9]

The QCSE creates band bending in the quantum wells (see Figure 3). Solving Schroedinger's equation for this sloped potential (and making use of effective mass approximations) gives electron and hole wave functions that are separated and pushed to opposite sides of the well. The reduced overlap results in a corresponding reduction in absorption and luminescence as well as an increase in the threshold current. Also, the energies of the bound states are decreased, resulting in reduced transition energy. Another substantial effect is the increase in the probability of electrons tunneling into the conduction band, resulting in a decrease in carrier lifetimes and a broadening of the spectra. In our structure we have a p-i-n junction that has an electric field in the intrinsic material. Applying a forward bias reduces this E-field, thereby countering the QCSE in the active region.

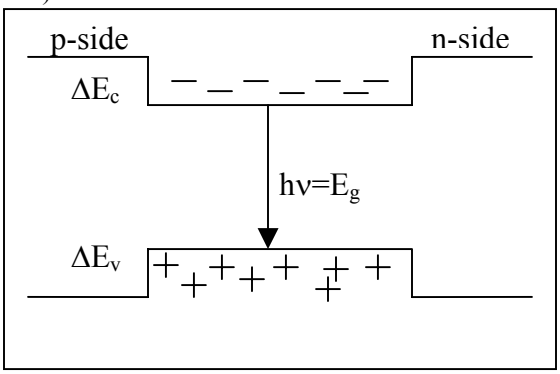

Fig. 2 – Schematic of double heterostructure band diagram at zero bias. Electrons and holes are confined in the well and recombine.

Phase Separation in InGaN

Phase separation is observed in X-ray diffraction (XRD) optical absorption measurements of InGaN.[10] XRD measurements of InGaN show peaks at separate phases for GaN and InGaN. However, an additional phase separated InN peak exists due to InN rich regions. These InN rich regions play a significant role in the emission mechanism of nitride based LEDs. The In rich regions affect GaN well layers by reducing the band gap across the well, as shown in Figure 4. The electrons and holes are confined in the In rich regions, hence the overlap is increased and recombination is enhanced, which in turn increases the emission intensity.

Also, the compositional fluctuation of InGaN in the quantum well is advantageous under polarization effects. As seen previously, there is a reduced overlap of electron and hole wave functions. However, the fluctuations have the effect of spreading the wave functions away from the corners of the well, thus increasing overlap and absorption. In addition, these variations in composition act as local centers of carrier confinement, thus increasing radiative recombination rates.

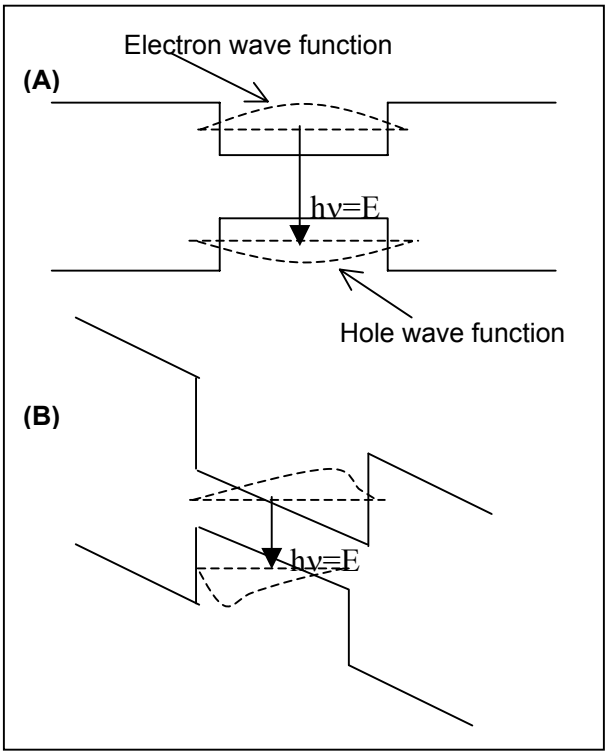

Fig. 3 – (A) Recombination in a quantum well in the absence of a piezoelectric field, and (B) in the presence of a transverse electric field where the Overlap of wavefunctions decreases.

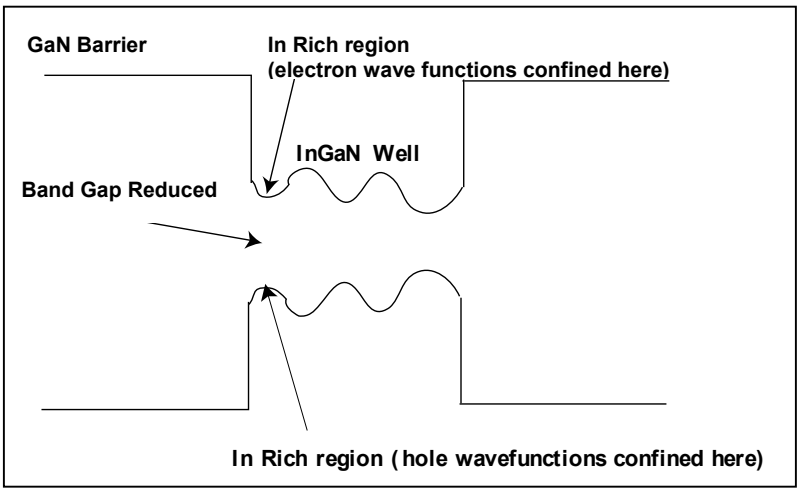

Fig. 4 – Band fluctuations in InGaN quantum well

II. Materials Growth and Characterization

Chemical Vapor Deposition (CVD) creates thin films of material on a substrate via the use of chemical reactions. Reactive gases are fed into a vacuum chamber and these gases react on a substrate and form a thin film or powder. As grown GaN films grown on a sapphire substrate by metal organic CVD (MOCVD) are n-type. Originally, a thin delivery tube was used to feed a reactant gas to the substrate for the purpose of obtaining high gas velocity. However, this made it very difficult to obtain a high quality film uniformly over the substrate due to convection currents.

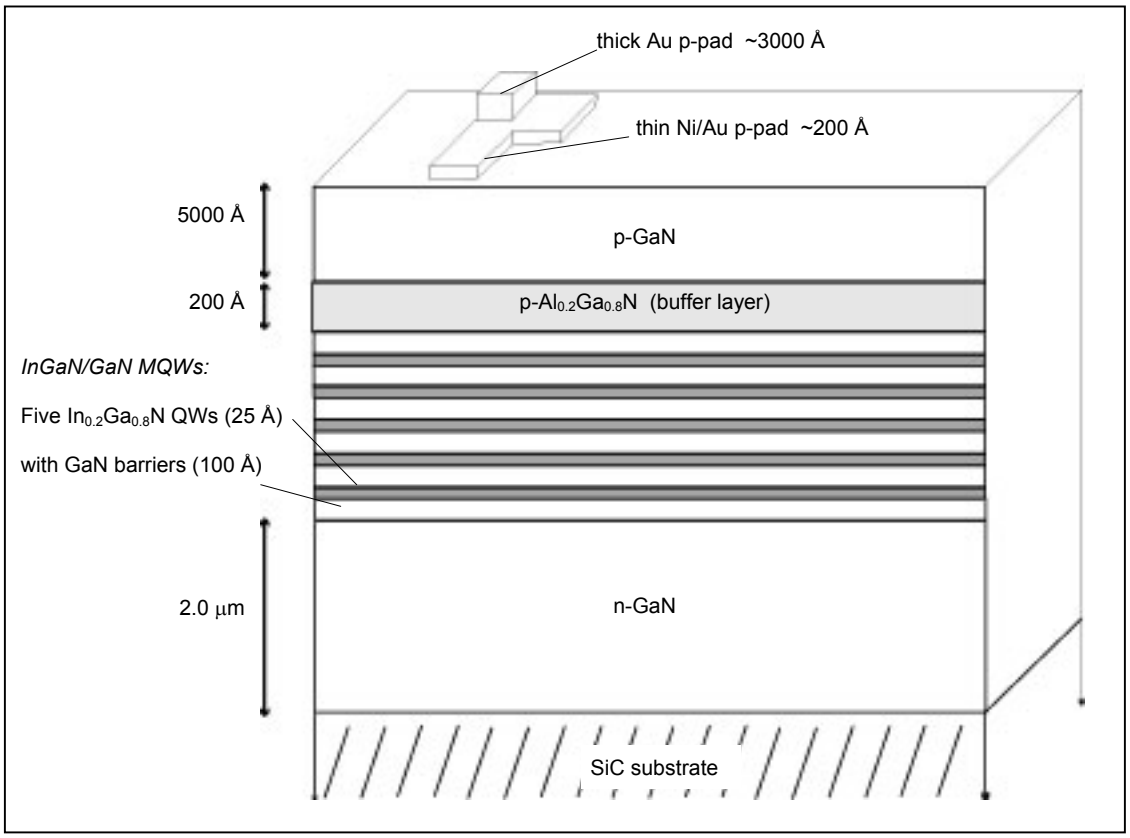

Fig. 5 – Blue InGaN/GaN MQW LED layer structure. The active region is composed of alternating InGaN quantum wells with GaN barriers.

A novel MOCVD reactor was developed by S. Nakamura that used two different gas flows: one is the main flow which carries the reactant gas parallel to the substrate with a high velocity.[11] The other is the sub flow which carries the inactive gas perpendicular to the substrate for the purpose of changing the direction of the main flow to bring the reactant gas into contact with the substrate. This subflow allows the formation of a continuous film as opposed to a few islands on the substrate. Usually a gas mixture of nitrogen or hydrogen is used as the subflow. This system is called a two flow MOCVD (TF-MOCVD).

Our samples were grown by MOCVD according to the layout in Figure 5. We were initially given half a wafer that had been grown up through the p-GaN layer – we only needed to deposit the Ni and Au contacts.

The n- and p-type GaN provide the necessary materials for the p-n junction. A perpetual difficulty when dealing with GaN is that there exists no lattice-matched substrate. Sapphire and Silicon Carbide (SiC) are frequently used due to their similar lattice constants (lattice mismatch of Sapphire = 13%, SiC = 3.5%), but defects due to threading dislocations are still a significant problem. Thin strained layers of GaN can be grown on Sapphire or SiC, but once the growth surpasses a critical thickness the strain relaxes and defects form at the interface. These dislocations thread throughout the entire growth of the material. In our case, 2.0 μm of n-GaN is far beyond the critical thickness, so the material contains a high concentration of defects that presumably hinder device performance. Fortunately, however, our SiC substrate is transparent to visible light. This allows light from our active region to escape in the downward direction. During packaging, the LED can be placed in a parabolic mirror casing so that this downward light can be refocused outward which greatly improves the extraction efficiency of the device.

The p-$Al_{0.2}Ga_{0.8}N$ layer acts as a buffer between the intrinsic GaN and the p-GaN. The energy band diagram (Figure 6) illustrates how this layer serves to block the free carriers and keep them more localized to the MQW active region.

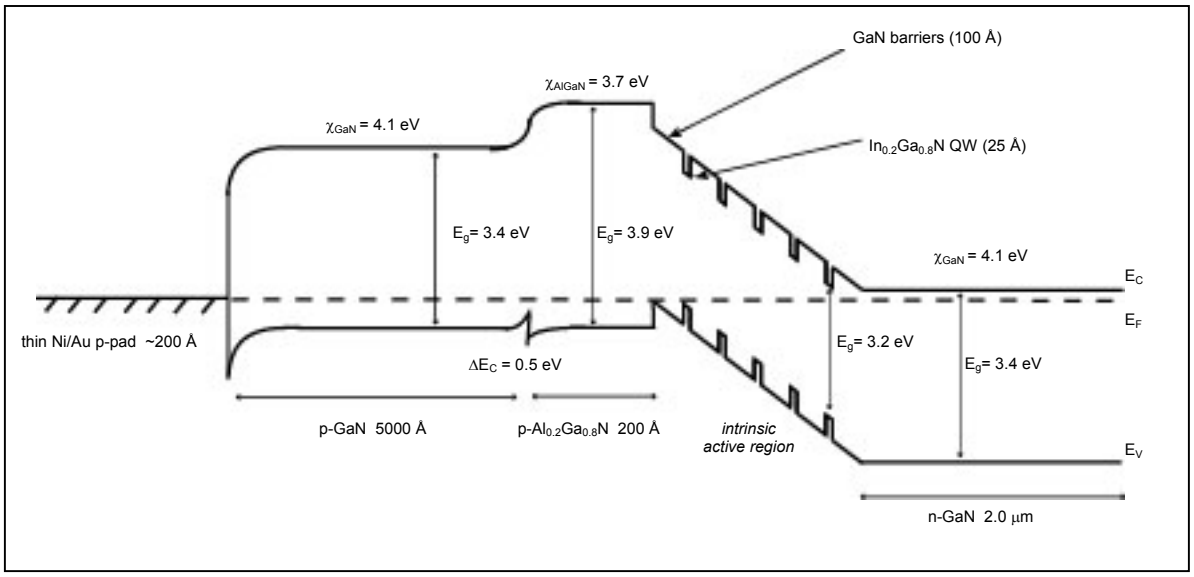

Fig. 6 – Energy band diagram for the InGaN MQW Blue LED.

The active region of our device is composed of alternating layers of $In_{0.2}Ga_{0.8}N$ and GaN. These layers were grown by MOCVD, with the 100 Å GaN layers acting as the barriers to the 25 Å $In_{0.2}Ga_{0.8}N$ quantum wells. This multi-quantum well (MQW) design provides strong carrier confinement which greatly enhances the spontaneous emission efficiency of the device (as discussed above).

The energy band diagram (Figure 6) does not account for net polarization effects which are, in fact, present in our device in the MQW intrinsic region. We suspect that this polarization (which is independent of applied bias) induces a QCSE which red shifts all spectral lines. A second QCSE exists due to the E-field in the intrinsic material which blue shifts the spectral lines; this effect can be modulated by forward biasing. The net effect is a sum of

these two effects, and thus we expect a blue shift with increasing current. Another salient feature of the band diagram is the Schottky barrier. The degree to which our Ni/Au contacts function as Schottky barriers or Ohmic contacts will be addressed in the discussion section.

All GaN, as grown by MOCVD, is n-type as a result of defects or impurities from the substrate (oxygen in the case of sapphire). P-type GaN, however, has been much more difficult to grow by MOCVD.[12] It was eventually realized that the magnesium acceptors were co-doping with passivating hydrogen which negated the acceptor's ability to generate free carriers. However, this co-doping effect is necessary because it lowers the formation energy so that it is possible to dope with the Mg acceptors. Therefore, the Mg acceptor dopants require activation by rapid thermal annealing (RTA); this removes the H and is known as the hydrogen desorption process. During the annealing, the hydrogen atoms which are interstitially bonded to the lattice break free and bond with the nitrogen atoms in the ambient N_2 gas. This removal of the interstitial H atoms is crucial to obtaining p-type GaN. As we will discuss later, H desorption also increases the hole concentration, which decreases the Schottky barrier width. This permits hole tunneling which causes the p-contacts to be more Ohmic.

It has been suggested that adding oxygen to the ambient gas mixture could further improve the Mg activation process.[13] Oxygen does not act as a donor, and thus it may more effectively remove H by allowing the formation of H_2O. It has been shown that annealing in N_2O enhances the activation of Mg acceptors and is more effective for getting high hole concentrations at lower annealing temperatures.[14]

In class it was reported that Ni can act as a catalyst to enhance H desorption at lower annealing temperatures (as low as 200°C).[15] It was thus concluded that the rate-limiting step of the H desorption process is the recombination reaction rate on the GaN:Mg surface, and its activation energy can be reduced by the Ni catalyst. Essentially, normal H desorption is limited by a surface barrier which can be reduced by the Ni.

RTA after deposition of Ni/Au contacts has been shown to cause a strange trading of places between the Ni and Au contact layers.[16] (This may also be related to a demonstrated agglomeration of the Ni film.) Further, the switch causes a unexpected surface morphology and apparent transparency that permits light to pass through the thin contact layer, thus improving efficiency. The details of this switching mechanism are addressed by Chen et al.[17] However, it has been suggested that oxygen assists the layer-reversal reactions of the metallized layers to form a structure of NiO/Au/p-GaN.[18]

From our visual inspection of the samples using a microscope, it was difficult to determine which thin p-contacts were transparent, and the degree of their transparency. It is therefore difficult to experimentally verify whether the RTA did, in fact, cause the Ni/Au position reversal and subsequent transparency.

After the initial wafer growth, the Mg acceptor dopant was activated in Samples #2A-B and #3A-B by Rapid Thermal Annealing (RTA) at 800°C for 5 min. Samples #1A and #1B were annealed after the deposition of the thin p-contact layers (see Table 1).

Table 1

Sample	when annealed	RTA temperature (°C)	RTA time (min.)	RTA ambient gas
first sample set processed during the week of 4/26/02				
1A	after thin p-pad deposition	800	5 min.	12% O_2, 88% N_2
2A	after GaN growth	800	5 min.	12% O_2, 88% N_2
3A	after GaN growth	800	5 min.	100% N_2
second sample set processed during the evening of 5/6/02				
1B	after thin p-pad deposition	800	5 min.	12% O_2, 88% N_2
2B	after GaN growth	800	5 min.	12% O_2, 88% N_2
3B	after GaN growth	800	5 min.	100% N_2

III. LED Fabrication – Processing

The processing of our samples followed the flowchart seen in Figure 7. This section will report any anomalous aspects of this processing, as well as the degree of difficulty or success encountered therein.

While performing several introductory tests with dummy Si wafers, we noted that the evacuation rate of the SRC 3176 metal evaporator was significantly less than that of SRC 3177. We therefore used the latter for the rest of our metal evaporation processes.

Due to the high cost of GaN wafers, we split our half wafer into 6 pieces: 3 pieces constituted the first group of samples (1A, 2A, 3A) that were fully processed during the week of 4/26/02 (see Table 1). The other 3 pieces were left as back up after the thin p-pad deposition; this was a prudent decision. As will be discussed, we were forced to make use of our second group of samples (1B, 2B, 3B) to achieve reasonable measurements during characterization.

We began processing all six samples by evaporating ~100 Å of Ni followed by ~100 Å of Au. After spinning Shipley 812 photoresist at 4000 rpm for 30 seconds, we exposed the samples under the transparent p-pad mask for 15 seconds. We then developed our samples in MF 321 for 60 seconds. This was followed by a 5 second Iodine immersion to etch the thin Au pads. The Ni pads were etched in Nitric acid for 10 seconds.

We then arrived at a "resting" point – we had to wait for Jae to anneal samples #1A and #1B. We used this opportunity to take a picture of sample #1A with only the thin p-pads (see Figure 8); this confirmed a relatively clean etching and surface morphology.

Upon receiving sample #1A after RTA, we noted a brownish tint on its surface compared to samples #2A and #3A which maintained their normal color. Unfortunately, this coloration was not apparent in the pictures produced.

We then proceeded to deposit the thick p-pads on our first set of samples (#1A, #2A, #3A). After spinning AZ 5214 photoresist at 4000 rpm for 30 seconds, we exposed the samples under the thick p-pad mask for 10 seconds. This was followed by a hardbake at 125°C for 65 seconds, and a 50 second flood exposure. We developed our samples in MF 701 for 60 seconds. We then evaporated ~3000 Å of Au for the thick p-pads. We generally found that, using tungsten boats, Ni evaporated at ~300 amps, while Au evaporated at ~ 150 amps. Upon inspecting our wafers after evaporation, we could clearly detect a deposition gradient across the metal panel inside the evaporator. The sample closest to the detector crystal (#1A) had the thinnest Au coating; the gradient increased with distance from the crystal. As our

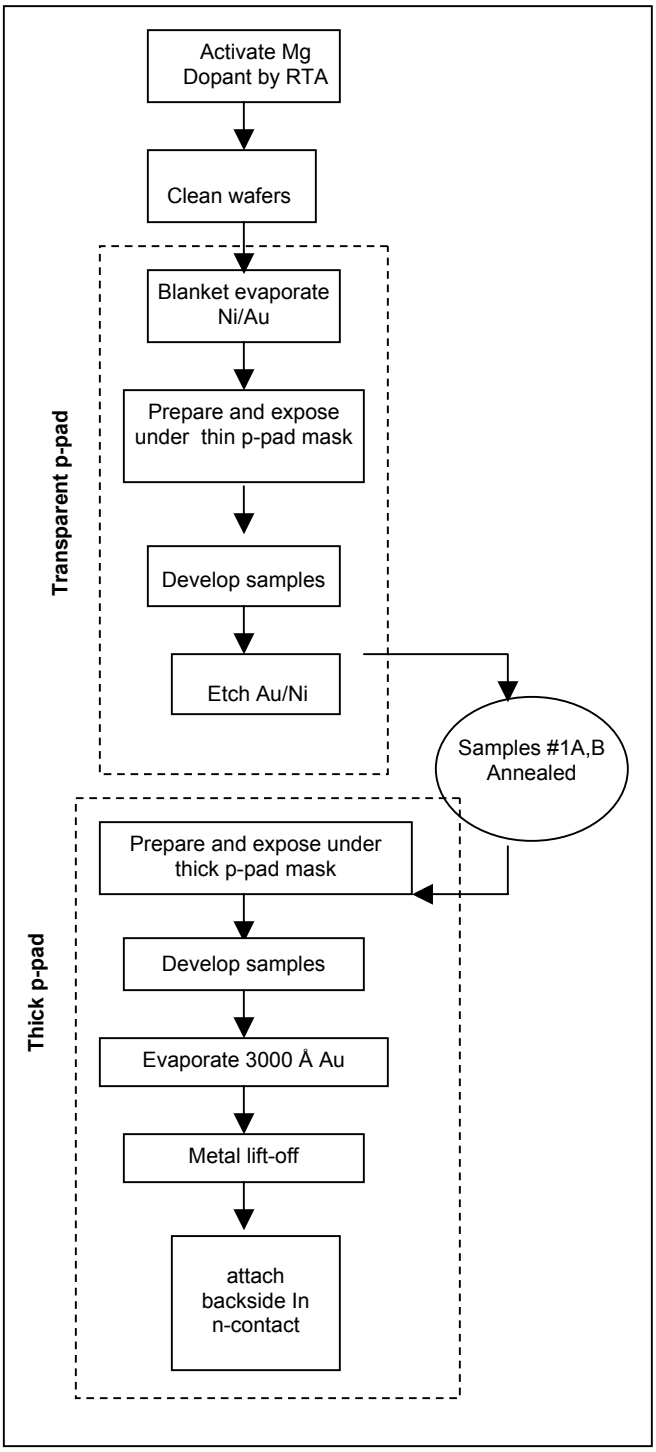

Fig. 7 – process flowchart

detector measured approximately 2500 Å, we can only presume that samples #2A and #3A were coated even more thickly, perhaps as much as 3000-4000 Å. We believe these differences became important during our liftoff steps.

We will now address the final step before device characterization – liftoff – in greater detail. Crucial to all of the photolithography steps is good photoresist dissolution at the very end of the process. This is normally accomplished by soaking the sample in Acetone which dissolves the photoresist layer and lifts off the layer of thick Au on top of it. In order to achieve a good liftoff, one hopes that there has been sufficient undercut during the exposure and the developing (see Figure 9).

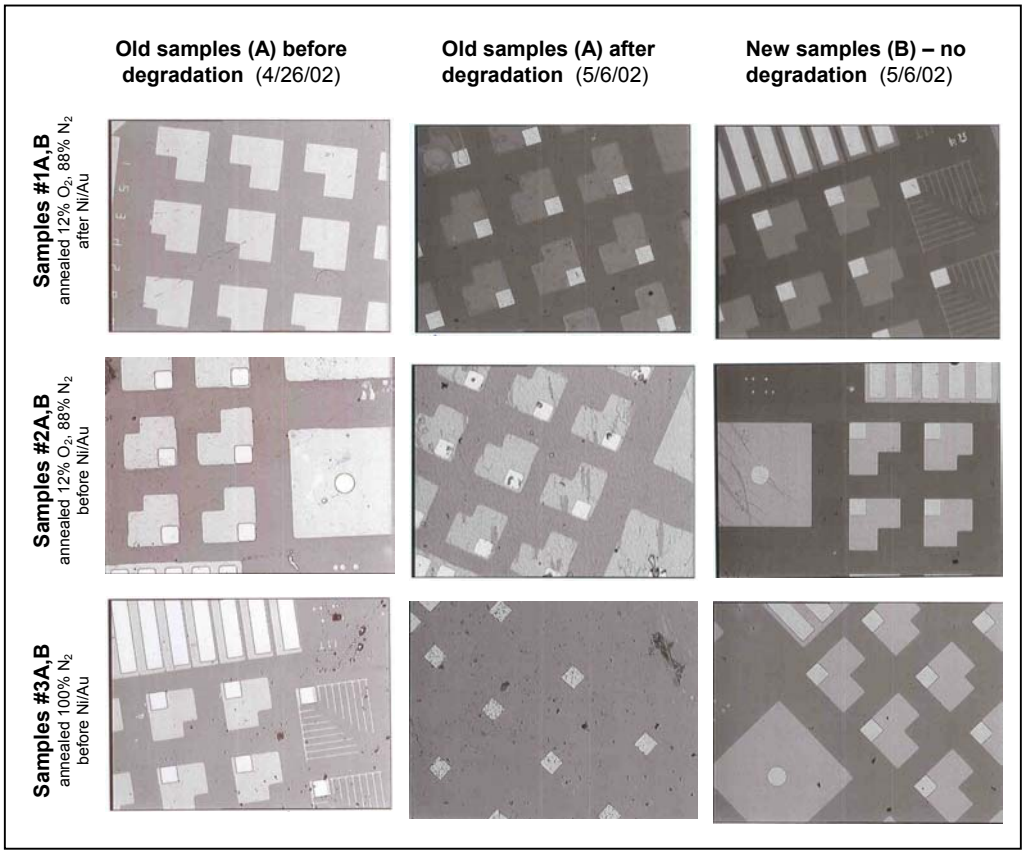

Fig. 8 – Sample sets shown at different times during processing. Initially, our first set of samples (A) showed good surface characteristics and alignment. After about 10 days, however, the surface was highly degraded. In sample #3A the thin p-pads had entirely and mysteriously disappeared. The second set of samples (B) showed excellent surface characteristics and alignment. Measurements were taken immediately before any degradation was possible.

In our case, however, the only sample that initially had a successful lift off was sample #3A. Upon soaking in Acetone for 3-4 minutes, the excess gold lifted off without difficulty. But we were forced to soak our other samples for much longer: #1A and #2A were immersed for ~ 5 hours, and even then the gold layers only lifted off with the assistance of a cotton swab to rub them off. Unfortunately, this also removed some of the thick p-pads from our samples but not enough to hinder any characterization efforts.

At first, it seems counterintuitive that the sample with the thickest deposition of Au (#3A with perhaps as much as 4000 Å) would lift off the most easily– one would expect that thinner layers of metal would be more prone to breaking contact with other metal and lifting off with the photoresist. However, we developed the following theory to explain what we observed: the expectation of good liftoff with thin metal layers assumes a good undercut (shown in Figure 9B). However, without a sufficient undercut, the deposition layer on top of the photoresist might look more like Figure 10C-D. Here it is seen that a thin layer of Au coats the photoresist in a fairly uniform fashion, with no obviously weak joints where the Au would be prone to break and liftoff. A thicker layer, however, might deposit such that weak joints exist around the edges of the photoresist so that as the sample soaks in Acetone and

the photoresist begins to "loosen," the greater mass of this thicker Au layer provides sufficient leverage and torque to break the weak joints and thus liftoff with the rest of the photoresist. Samples #1A and #2A ultimately lifted and pictures of their surfaces and the thick p-pads are seen in Figure 8.

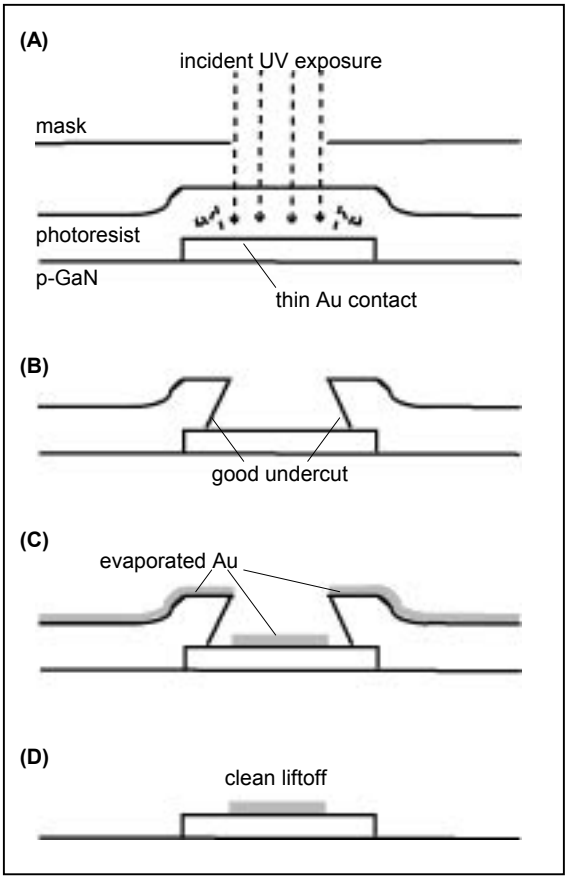

Fig. 9 – (A) Photoresist being exposed to UV light – reflected rays expose areas of PR not directly under column of exposure. (B) Subsequently, a good undercut profile is achieved after developing. (C) Au is evaporated onto the surface in a line-of-sight fashion, enabling a break between pieces of evaporated Au. (D) These breaks facilitate clean liftoff in Acetone.

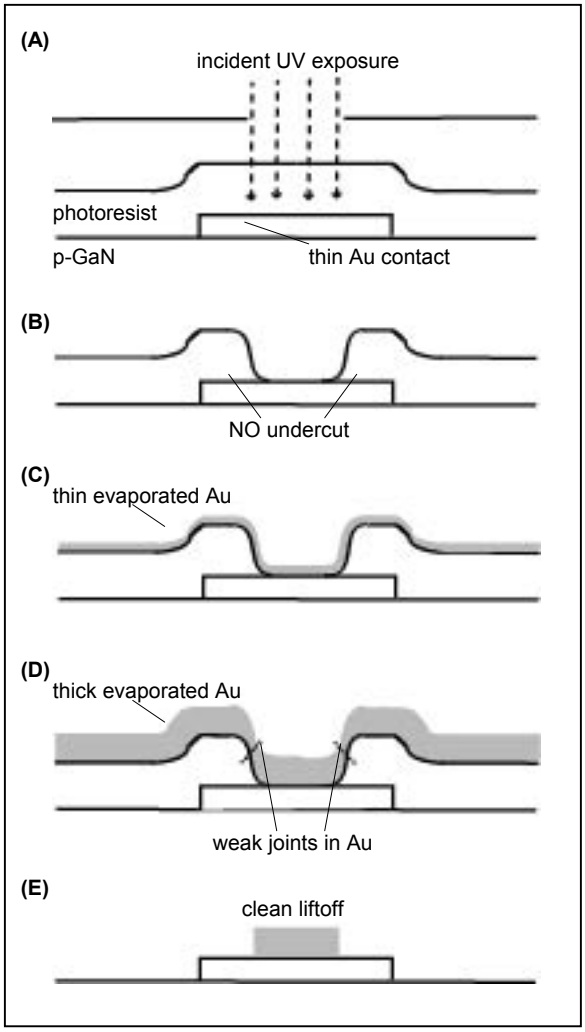

Fig. 10 – (A)-(B) exposure to UV rays does not provide sufficient undercut. (C) Thin Au has no weak joints. (D) Line-of-sight deposited thick Au has weaker joints that break when Acetone lifts off PR, thus giving (E) a clean liftoff

Indium solder contacts were then attached to the undersides of all three samples. The samples were then ready for characterization. However, as will be further detailed in the discussion section, our first set of samples suffered significant degradation over a period of roughly 10 days – enough so that output power and spectral measurements were impossible to achieve with samples #2A and #3A. When this was discovered, we took another set of pictures to verify the condition of our samples' surfaces (see Figure 8). Degradation can clearly be seen. Sample #1A was the least affected of the three; it continued to luminesce even after #2A and #3A were all but unusable. Sample #2A showed marked scratches on the thin p-pads, and many were beginning to fall off. Sample #3A was by far the worst – its picture reveals that all of the thin p-pads were completely gone. This is a strange phenomenon, but possibly just an extension of what was beginning to happen to sample #2A. Reasons for the degradation are numerous, ranging from careless wafer handling (accidental scratches with tweezers or probes), to interaction with the non-cleanroom laboratory environment in which we made our measurements. At this time, it is

not understood why the degradation affected some wafers more strongly than others.

Because the degradation of samples #2A and #3A had rendered them useless for the vital aspects of characterization, we finished processing our second set of samples (#1B, #2B, and #3B). Having left off just after the deposition of the thin p-pads, we proceeded with the deposition of the thick p-pads. After spinning AZ 5214 photoresist at 4000 rpm for 30 seconds, we exposed the samples under the thick p-pad mask for 10 seconds. This was followed by a hardbake at 125°C for 65 seconds, and a 50 second flood exposure. We developed our samples in MF 701 for 60 seconds.

Based on our experience evaporating the thick p-pads for our first set of samples, we determined that to accommodate the best metal lift-off, we should try to deposit very thick layers of Au. We positioned all three samples very close together on the underside of the metal evaporator plate to try to achieve uniform thickness on all three wafers. We then evaporated ~3700 Å of Au for the thick p-pads.

Metal liftoff was subsequently easy, potentially validating our liftoff theory for thick Au deposition. All three samples lifted off with ~ 5 min. of soaking in Acetone and only minimal cotton swabbing around the edges of the samples. We took pictures of all three samples at this point (see Figure 8). Their surface characteristics were excellent – the contacts were very sharply defined and well aligned. There was very little dust on the surfaces and there were a large number of usable contacts for characterization. At that time, there was no degradation evident whatsoever; thus we thought it wise to make all of our measurements as quickly as possible after the initial processing. (Additionally, doing all of our measurements at once would guarantee non-varying equipment setup and conditions.) Indium solder contacts were then attached to the undersides of all three samples (#1B, #2B, and #3B).

IV. Device Characterization – Results and Discussion

Characterization of the LEDs was done on a probe station with a curve tracer, an optical spectrum analyzer and a photometer. All measurements except contact resistance were carried out on the small 300 square micron LED pads. Contact resistance was obtained using transverse length modulation (TLM) on a test structure with pad widths of 1000 μm and varying distances between the pads.

A curve tracer powered the LEDs for spectra and power measurements. As set up, the curve tracer provided an AC current that reverse and forward biased the junction. This caused two problems: first, the reverse bias swing seemed to hasten the deterioration of the samples. In addition, this caused what looked like sub-band transitions in the spectra measurements. The superposition of the AC drive current and sweep rate in the optical spectrum analyzer caused these fringes. We found and reported that using a DC drive current fixed these problems and took our measurements with this setup. Our samples' output power vs. current is presented in Figure 11. From the L-I curves, it is apparent that the RTA did not affect the efficiency of our samples' transparent *p*-pads. For samples with pads deposited after annealing (ambient O_2N_2), the power was essentially the same as if the pads had been deposited before activation. It is also apparent from the L-I curves that

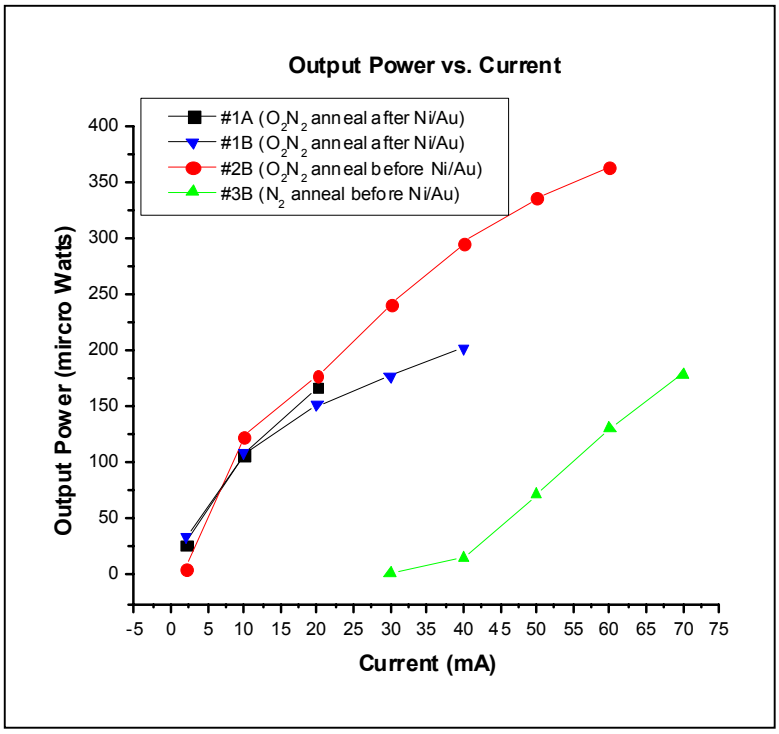

Fig. 11 – Output power vs. current for the second set of samples (#1B, #2B, #3B) and the only functioning sample from the first set (#1A). Note that the highest output power was actually achieved with the sample that was annealed before thick p-pad deposition.

nitrogen annealing is not an effective hydrogen getter since the output power was low and the samples had extremely low power efficiency.

Several factors may have contributed to the poor transparent *p*-pad quality on all of our samples. The thin pads were deposited using a two step process that allow the atmosphere to come into contact with the nickel before any gold was evaporated. This would have oxidized the nickel, and may have made the RTA less effective. Knowing this, the metals should be evaporated without breaking the vacuum to prevent the nickel from oxidizing.

Another factor that may have contributed to the poor quality of the contacts is that the entire half wafer did not seem to be uniform. The lack of uniformity may suggest that samples #1A and #1B (annealed after thin p-pad deposition) had more defects than samples #2A and #2B that were annealed in $12\%O_2 88\%N_2$ before any metal was deposited. In this case, the annealing may have been successful, but the presence of the defects would negate any benefit provided by the RTA.

The output spectra of the LEDs are presented in Figures 12, 13 and 14. A set of emission spectra for low current densities could not be obtained for sample #3B (RTA in N_2 ambient) due to the LED's low efficiency. Figure 12 shows the emission spectra for the second set of samples, as well as sample #1A from the first set. These spectra were measured at 20mA, except for sample #3B, which did not have measurable power or a clean spectrum below 80mA. The difference in peak wavelengths could be attributed to differences in quantum well thickness throughout the GaN wafer. This is apparent when comparing the center wavelengths of samples #1A and #1B which were processed nearly identically and are both from the same wafer, having only been split before processing.

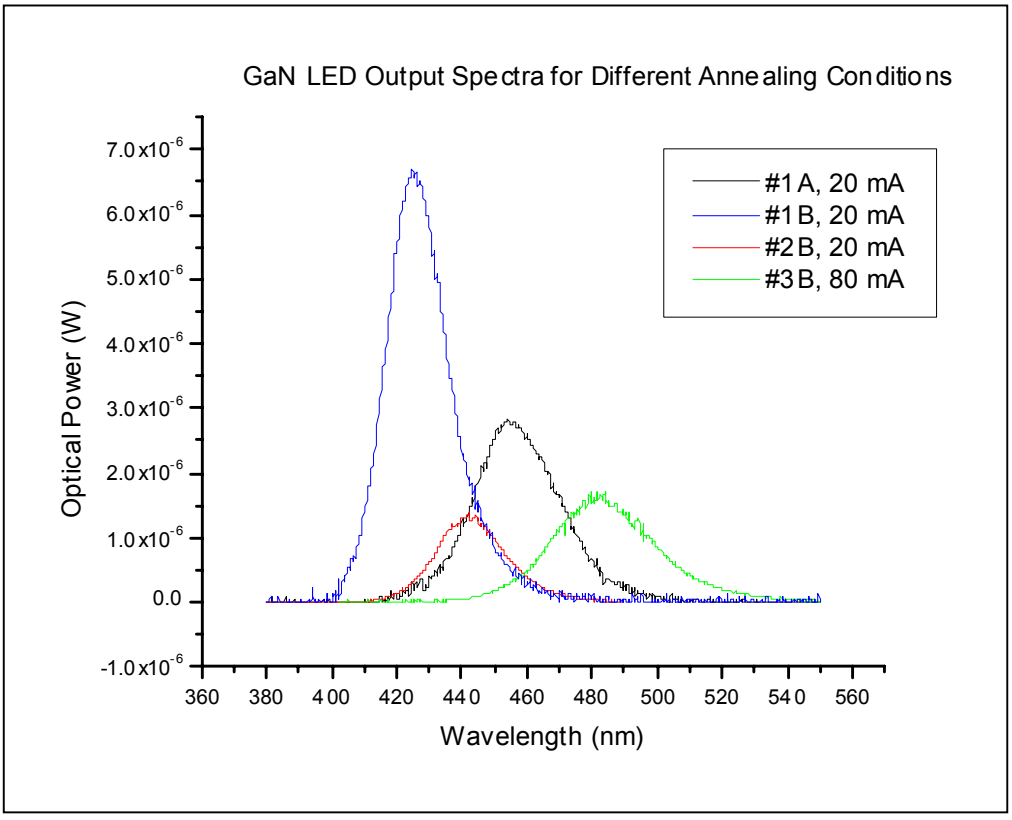

Fig. 12 – Output spectra for samples #1A, #1B, #2B and #3B. We did not see any noticeable emission ~ 550 nm (the characteristic deep level yellow luminescence), which would indicate that the deep donor levels (Ga or N vacancies) which normally cause this kind of emission are not present in our samples.

Figure 13 shows the spectrum for sample #1A (first set RTA in N_2O_2 after thin p-pad deposition). Noteworthy is the lower power output at 20mA than 10mA. This is due to a rapid deterioration of the sample at higher current densities. This deterioration is likely in the p-type contact, as the emission spectrum did not

appreciably change in shape. Not all of the samples demonstrated this behavior, so the deterioration may be encouraged by differences in the epitaxial layer structure. The spectra shows a blue shift at higher current densities. The shift from 2mA to 10mA is 3nm. It has been suggested that the blue shift of the spectra peak with increasing current is a result of the QCSE, which in turn is due to the E-field in the intrinsic InGaN quantum wells.[19] We postulate that the shift we observed is due to the reduction of the electric field in the active region, thereby reducing the QCSE in the quantum wells. We note that growth on the M- or A- planes of GaN would eliminate this spontaneous piezoelectric polarization.

Figures 14 demonstrates this same effect for sample #2B; note that the sample did not deteriorate for higher current densities as demonstrated by the increasing intensity with increasing current.

As mentioned, the wafers did not seem to be uniformly grown. The spectra in Figure 12 show this, and Table 2 shows the variation in output power by position for sample #1A. For probe position, "left" indicates toward the center of the half-wafer as grown, and "right" is toward the outer edge. On the right, the LED rapidly deteriorated – its light was not visible for any length of time, though it still passed current. This seems to suggest a faulty epitaxial layer structure, but could also suggest some variation of pad quality. While not measured due to low power output, the spectra of the samples clearly varied, with the LEDs near the edge being more blue and violet than those near the center (which were almost teal colored). This strengthens the theory that the epilayers were not uniform since a blue shift indicates either a lower electric field or a thinner quantum well. The amount of blue shift is quite large as seen in Figures 13 and 14, suggesting that the quantum wells may have been grown thinner toward the edges of the wafer. Table 3 shows the peak wavelengths and FWHMs for our samples.

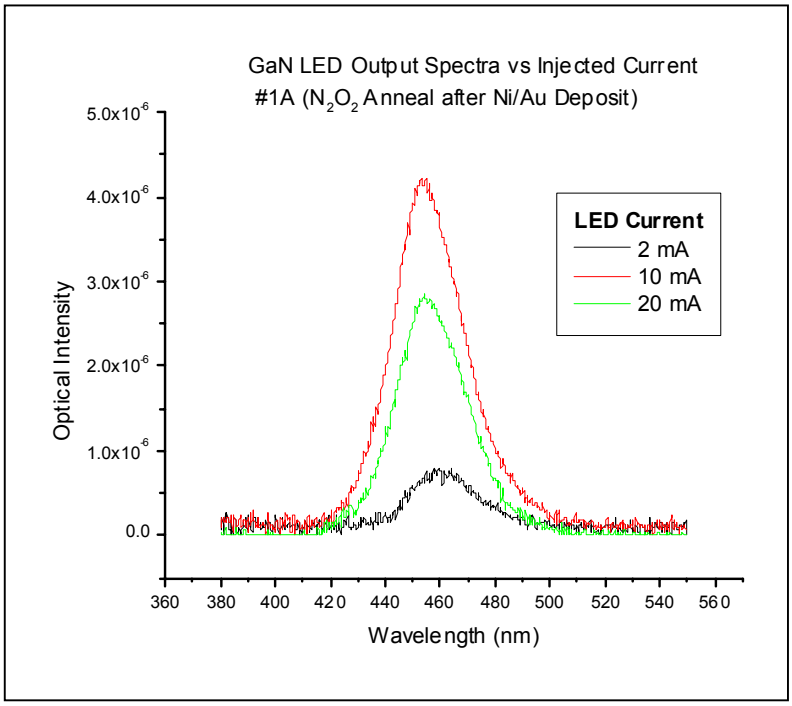

Fig. 13 – Sample #1A output spectra vs. injected current. A blue-shift can be seen for increasing current.

Table 2

probe position on wafer	current (mA)	output power (μW)
left	20	163.6
middle	20	45.4
right	20	break down, no power out

The hypothetical external quantum efficiencies for the LEDs are shown in Figure 15. The hypothetical external quantum efficiency in this case is simply the measured efficiency multiplied by a factor of six. This assumes that the LED could be made sufficiently small and pads small enough to extract all of the light. The efficiency drops with increased current, which may suggest increased carrier leakage out of the active region.

The current-voltage (I-V) measurements are shown in Figure 16. Values for the series resistance, R_S, were obtained from this plot. The resistance of the N_2O_2 RTA samples is clearly the lowest, indicating a higher quality *p*-contact. The turn on voltages for the samples that were annealed before metal deposition are 4.2V for sample #3B (N_2 RTA) and 4.8V for sample #2B (N_2O_2 RTA). These are roughly what was expected. However, the sample that had metal deposited before RTA (sample #1B) had a very high turn-on voltage. This varied from LED to LED, but

was typically about 11V. This may be due to the fact that this samples' set of contacts were more like Schottky barriers than Ohmic contacts.

High contact resistance of p-GaN contacts is a significant problem. There are traditionally only two ways to decrease this contact resistance: higher p-type doping (which is very difficult to achieve in GaN) or lowering of the Schottky barrier until it is effectively Ohmic. Since it has, to date, been impossible to find a p-type GaN contact metal with a work function $\phi_M \geq \phi_S$ (the necessary condition for the removal of the barrier $q\phi_B$), we must resort to barrier manipulation to achieve the most Ohmic contact possible. This is achieved through p-type doping which reduces the depletion width and barrier thickness as seen in Figure 17. It was reported that tunneling occurs freely for doping concentrations of $N_A \geq 10^{18}$, where barrier thickness $W \propto N_A^{-\frac{1}{2}}$.[20] Additionally, impurity defects at the Ni-GaN:Mg interface create a "leaky" Schottky barrier which enables more holes to transit across the barrier, thus enabling higher current densities and making the contact more Ohmic.

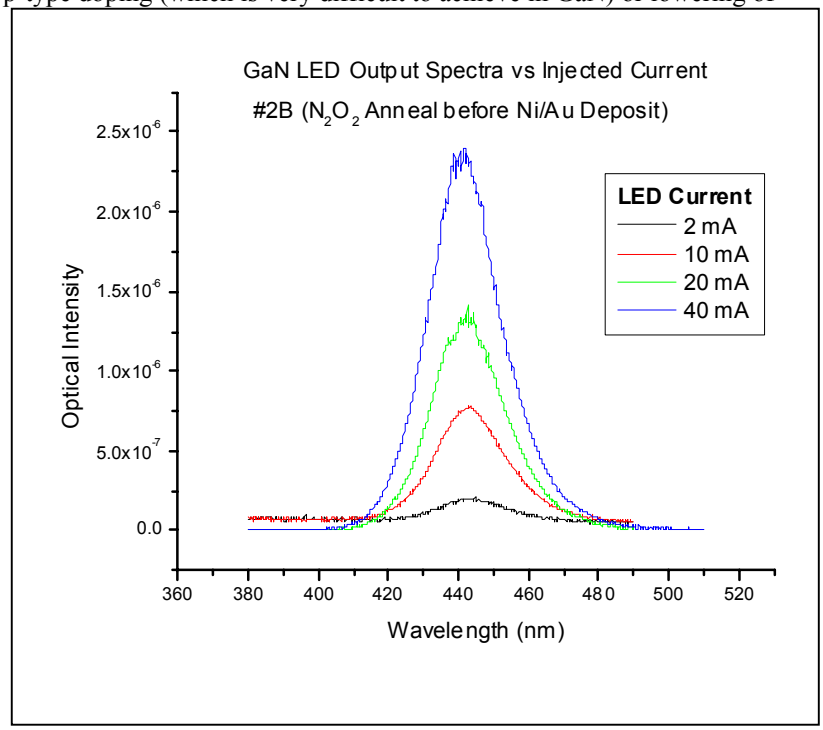

Fig. 14 – output spectra vs. injected current for sample #2B. A blue shift is noted for increasing current.

Thus we would have hoped that the RTA performed on our samples had activated the Mg, increased the p-type doping, decreased the depletion width of the Schottky barrier contacts, and increased the ability of carriers to tunnel, thereby making our contacts more Ohmic. It is not entirely clear whether this was realized in our case – as will be seen, we measured extremely high contact resistances and somewhat high values for series resistances. This could have been due to the SiC substrate, but we suspect our contacts are a Schottky-Ohmic hybrid.

The contact resistances of our samples were measured using TLM on a test pattern that was 1000 microns wide with separations of 20, 15, 10, 8, 6 and 5 microns. Due to poor lithography, some of the wafers did not have all of the available separations. Also, the measurements were typically made far away from the high quality areas of the wafer because the TLM patterns were not local to the small LED pads that yielded good spectra, I-V, and power measurements. This leads to data that is most likely not indicative of devices under operation. In fact, the resistances were so high that they clearly eclipsed the measured series resistances. The sheet resistances are also shown in Table 4. These numbers seem to indicate a problem

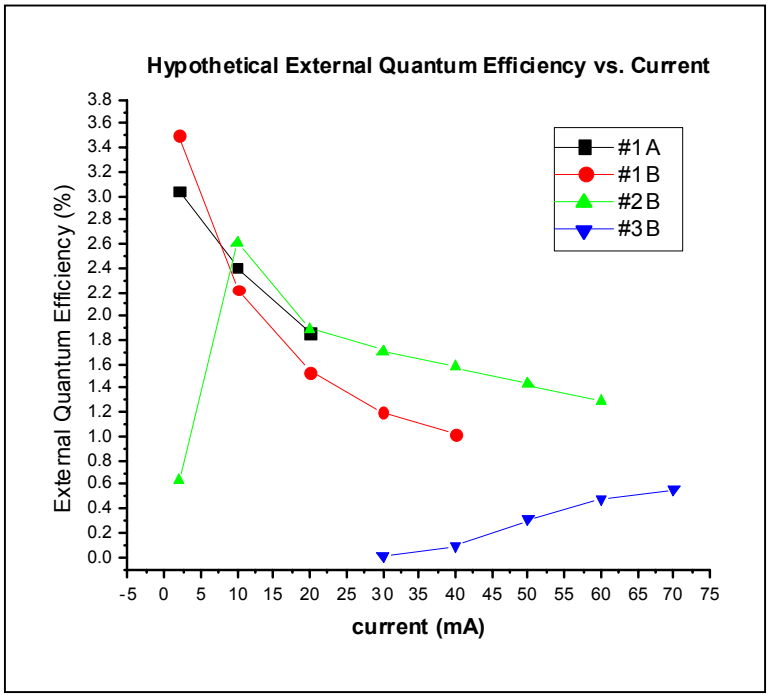

Fig. 15 – Hypothetical External Quantum Efficiency vs. Current for four samples.

with our pads for TLM, but if taken as they are, they show that the sheet resistance for the *p*-GaN is lowest in sample #1B (annealed after metal deposition). It also shows that sample #1A (first set of samples) had degraded. It is doubtful, however, that the material degraded to the degree shown unless it can be attributed to variation in the wafer growth. It would seem that only the contacts would degrade, which would not affect the sheet resistance. Therefore, the poor measurements may be attributed to the lithography quality of the pads and should not be trusted. To improve our contact resistance measurements, we could have used a four point probe to measure the sheet resistance of the *p*-GaN to verify resistances measured using TLM.

A contact resistance of $R_0 \sim 2*10^4\ \Omega$ has been reported for an Ni/Au contact on p-type GaN, and R_0 decreased to $\sim 0.5*10^4\ \Omega$ after annealing in N_2/O_2 ambient at 500°C.[21] Our results are clearly much higher than reported measurements; this gives further reason to question our results.

Table 3

sample	current (mA)	peak wavelength (nm)	FWHM (nm)
1A	2	461.7	26.7
1A	10	455.8	29.6
1A	20	456.8	29.6
1B	2	429.7	20.5
1B	10	426.7	21.0
1B	20	426.2	21.8
2B	2	441.0	22.0
2B	10	443.6	24.0
2B	20	442.6	22.8
2B	40	441.4	23.6
3B	80	482.9	33.4

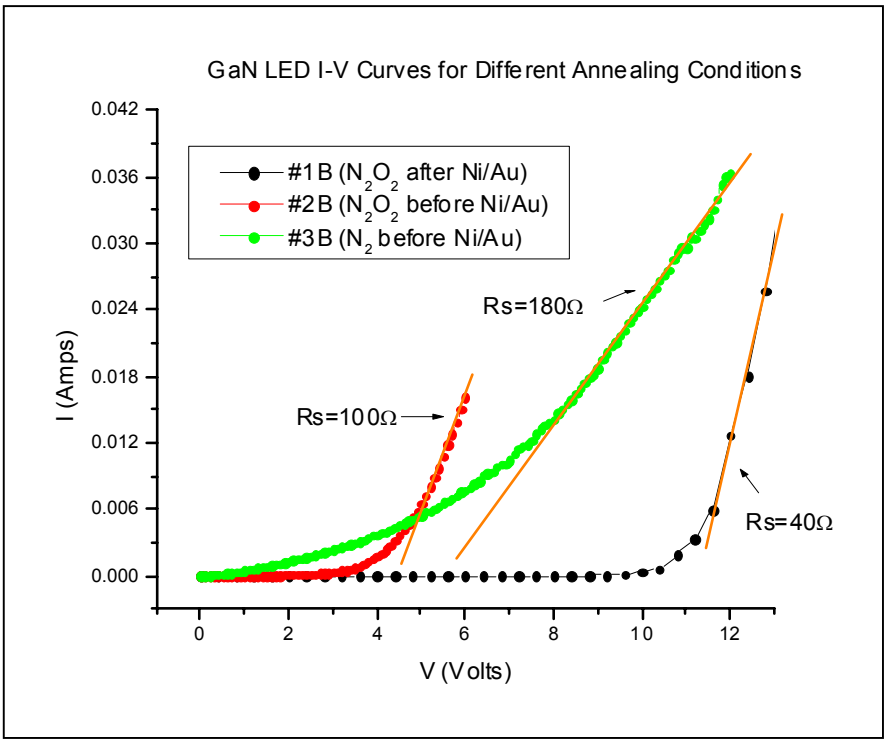

Fig. 16 – I-V curves for the second set of samples, #1B, #2B, and #3B.

Table 4		
Sample	Contact Resistance (MΩ)	Sheet Resistance (Ω/□)
1A	2.39	$2.3*10^8$
1B	2.30	14
2B	0.40	$7.38*10^6$
3B	5 (ohms) bad measurement?	98

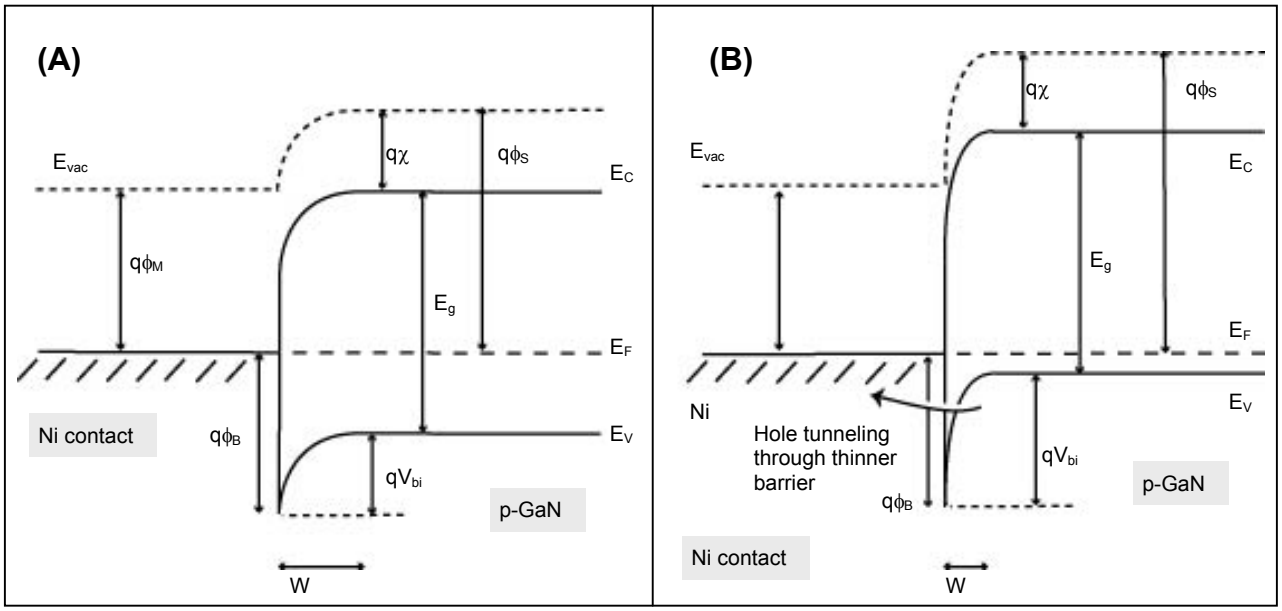

Fig. 17 -- A) Nickel contact with p-type GaN. Magnesium dopant has not been activated. There is a significant barrier to hole flow, and thus this is a Schottky barrier. B) With the removal of Hydrogen, the Mg acts as a full acceptor, and thus the effective doping concentration N_A increases. This shifts the band with respect to the Fermi level (as shown). Additionally, the higher doping concentration decreases the depletion width W. This decrease makes the barrier to holes much thinner and permits tunneling; the contact is then more Ohmic.

V. Conclusions

Several improvements could have been made to optical measuring techniques used to characterize the LEDs. For power output measurements, the placement of the photodiode had a huge affect on the power readings. Also, the photodiode we used only captured light from one output cone, so external quantum efficiency could not be calculated well. This could be improved with better backside contacting, using some sort of parabolic collector and proper collimating optics. Also, the spectra at low current densities could not be measured well due to poor coupling between the fiber and the sample. The peak powers of 300 μW were measured; however, only about 10 nW/nm were coupled into the optical spectrum analyzer. With a FWHM of 25nm, the maximum coupled power may have been about 2.5 μW, or about 1/100 of the incident power. A simple achromat lens would improve measurements by collimating and focusing the light on the fiber to increase coupled power.

We have presented the theory, fabrication, processing and characterization of an GaN/InGaN MQW LED. The MQW structure was chosen to increase internal quantum efficiency and fabricated by MOCVD using a SiC substrate. The *p*-type GaN was activated using various RTA steps with different ambient gases. Ohmic contacts

were deposited on the epilayer structure using evaporation, etching and liftoff. Various characteristics of the LEDs were measured including output power, contact resistance, sheet resistance of the *p*-GaN, and output spectra. In addition, the quality of the epitaxial layers was qualitatively evaluated using output spectra, I-V curves and visual cues. RTA with N_2O_2 was the most effective activation technique; we were not able to conclude, however, whether evaporating the Ni/Au thin p-pads before the RTA was the best method.

References

[1] Bhattacharya, P. (1997*). Semiconductor Optoelectronic Devices*. 2nd ed. Prentice Hall
[2] (ibid.)
[3] (ibid.)
[4] (ibid.)
[5] Nakamura, S. (2002). *220C In Class Lecture notes 3*. University of California, Santa Barbara
[6] (ibid.)
[7] Bhattacharya, P. (1997*). Semiconductor Optoelectronic Devices*. 2nd ed. Prentice Hall
[8] Nakamura, S. Pearton, D. Fasol, G. *The Blue Laser Diode: the complete story,* 2nd ed. Springer Press
[9] Davies, J. (2000). *The Physics of low dimensional semiconductors.* Cambridge University Press
[10] Singh, R. Doppalapudi, D. Mousatakas, T. (1997) Phase separation in InGaN thick films and formation of InGaN/GaN double heterostructures in the entire allow composition. *Appl. Phys. Lett 70 (9)*
[11] Nakamura, S. Pearton, D. Fasol, G. *The Blue Laser Diode: the complete story,* 2nd ed. Springer Press
[12] Nakamura, S. (2002). *220C In Class Lecture notes 3*. University of California, Santa Barbara
[13] (ibid.)
[14] (ibid.)
[15] (ibid.)
[16] (ibid.)
[17] Chen et al., J. App. Phys. **7**, 86, (1999)
[18] Qiao et al., J. App. Phys. **7**, 88 (2000)
[19] Takeuchi et al., J. App. Phys., 36 (1997)
[20] In Class Lecture Notes 3
[21] In Class Lecture Notes 4, after Koide et al., J. Electron. Mat. **28**, 341 (1999)